LAWRENCE
LIVERMORE
NATIONAL
LABORATORY

LLNL-JRNL-800865-DRAFT

# Role of opacity at the 9 keV back lighter energy used in measuring the equation of state of boron at pressures up to a Gbar

J. Nilsen, D. Aberg, H. D. Whitley, B. G. Wilson, L. H. Yang, P. A. Sterne, M. W. Daene, M. E. Martin, S. Zhang, W. R. Johnson

January 9, 2020

High Energy Density Physics

## Disclaimer

# Role of opacity at the 9 keV back lighter energy used in measuring the equation of state of boron at pressures up to a Gbar

Joseph Nilsen[1], Daniel Aberg[1], Heather D. Whitley[1], Brian G. Wilson[1], Lin H. Yang[1], Philip A. Sterne[1], Markus W. Daene[1], Madison E. Martin[1], Shuai Zhang[2], and Walter R. Johnson[3]

[1]*Lawrence Livermore National Laboratory, Livermore, CA 94551*
[2]*University of Rochester, Rochester, NY 14627*
[3]*University of Notre Dame, Notre Dame, IN 46556*

**Abstract.** Many experiments have been done at the National Ignition Facility to measure the equation of state Hugoniot of plastic, boron, and diamond at extreme pressures up to a Gbar. The "Gbar" design employs a strong spherically converging shock launched through a solid ball of material using a hohlraum radiation drive. The shock front conditions are characterized using X-ray radiography, typically at energies near 9 keV. In this paper we look at how the opacity of boron at 9 keV changes at high pressures and temperatures. Understanding this is vital to unfolding the density in the shock front as pressures exceed 100 Mbar. We compare opacity results between a number of methods including the legacy XSN opacity tables, super transition array (STA), average atom (AVAT), and detailed configuration accounting (DCA) methods. We examine how the changing opacity is correlated with the K-shell occupation calculated using the opacity methods as well as density functional theory (DFT) methods such as MECCA, Purgatorio, and an optimized all-electron pseudopotential theory (ONCV). We also examine the relative contribution of free-free opacity to the overall opacity that is dominated by bound-free absorption.

**Keywords:** Hugoniot, Opacity, Boron, Gbar

## 1. Introduction

Understanding matter at high energy density is of great importance in understanding ablators used in inertial confinement fusion (ICF) experiments and understanding the structure and evolution of astrophysical objects such as gas-giant planets, brown dwarfs, and highly evolved stars material where extreme pressures can exceed 100 Mbar and reach well into the Gbar regime [1-3]. At Lawrence Livermore National Laboratory (LLNL) the Gbar experimental platform has been developed and demonstrated [4-6] to study the shock compression (Hugoniot) of material compressed to near Gbar pressures in a spherically converging geometry using streaked X-ray radiography. In these experiments, the National Ignition Facility (NIF) laser heats the inside of a gold hohlraum and creates an X-ray radiation drive which ablates an outer ablator and sends a strong spherical shock into a solid sphere of material. The shock velocity and the density jump at the shock front are characterized using X-ray radiography to determine the pressure and density along the shock Hugoniot as the shock travels to the center of the solid sphere. As the shock travels toward the center the pressure increases like ~1/radius and the temperature at the shock front

increases, accordingly. Radiography measures the transmission through the target which is determined by knowing the integrated product of density ρ and opacity κ at the back-lighter energy. Recent experiments have measured the Hugoniot of CH plastic from 20 – 60 Mbar in a low-drive (300 kJ) NIF experiment [5,6] as well as boron and diamond. The Hugoniot gives the relation between pressure and density at the shock front for a strong single shock wave passing through the material. In the low-drive experiments below 100 Mbar the opacity of the material at the back-lighter energy, which is 9 keV for the CH and boron experiments, is the same as the cold opacity tabulated at LBL [7]. This is because the opacity of these materials is dominated by the K-shell (1s) electrons and at these low pressures the K-shell is fully occupied. However other experiments have measured the Hugoniot of CH, boron and diamond at pressures between 100 and 1000 Mbar in high-drive NIF experiments. See Ref. 8 for recent CH experiments. As the pressure exceeds 100 Mbar the materials start ionizing into the K-shell and the opacity of the materials at the back-lighter energy starts to fall. Since radiography measures the product of density and opacity it is vital to understand the opacity in order to unfold the density at the shock front to measure the Hugoniot of the material. In this paper we look at the opacity of boron at the 9 keV energy of the Zn He-α back-lighter and compare the opacity calculated between a number of methods including the XSN opacity tables [9-11] used at LLNL, super transition array (STA) methods [12-14], the average atom (AVAT) method used at Notre Dame [15,16], and detailed configuration accounting (DCA) methods [17,18]. We examine how the changing opacity is correlated with the K-shell occupation and also examine the relative contribution of free-free opacity to the overall opacity that is dominated by bound-free absorption. In addition to the opacity methods we calculate the K-shell occupation with density functional theory (DFT) methods such as MECCA [19,20], Purgatorio (PURGV) [21,22], and an optimized all-electron pseudopotential (ONCV) approach [23-25]. Since the density along the Hugoniot at the high pressures measured in our EOS experiments quickly reach densities near four times compressed we simplify many of the comparisons by looking at the opacity and K-shell occupation versus temperature for four times compressed boron. We focus on boron because it is a single material but all the same issues apply to materials such as plastic and diamond used in the Gbar experiments. Things become more complicated when one looks at compounds such as plastics because then one needs to address the issue of how to model mixtures, which will be discussed in a future publication.

## 2. Role of opacity in radiography on Gbar equation of state (EOS) experiments

The Gbar experimental platform is described in more detail in Refs. 4-6 but we give a brief overview of the recent experiments to measure the equation of state (EOS) of poly(α-methylstyrene) $C_9H_{10}$ plastic (PAMS) at pressures from 20 – 400 Mbar. The boron experiments use a very similar geometry and will be published in the future. In these experiments, solid targets are compressed and heated in an indirect drive laser geometry using 176 laser beams incident on an Au hohlraum. The CH targets consisted of solid CH spheres 970 μm in radius covered by a 185 μm thick plastic ablator made of glow-discharge polymer (GDP) with a graded Ge (Z=32) dopant. The Ge dopant serves as both a marker layer [6] in the experiment for the radiography as well as a preheat shield to reduce preheat of the plastic target. The role of preheat is discussed in detail in Ref. 26.

The CH experiments use a standard NIC scale 5.75 mm hohlraum (diameter = 5.75 mm and height = 9.42 mm) with a 0.03 mg/cc $^4$He gas fill and 3.375 mm diameter laser entrance hole. The hohlraum is driven by 176, 351-nm laser beams. For the low-drive experiments [5,6] the pulse shape is a 4-ns long, nearly square pulse with power of 78 TW. The total drive energy and power incident on the hohlraum walls is about ≅ 300 kJ for the low-drive experiments and 1.2 MJ for the high drive experiments. These drive conditions result in a predicted peak hohlraum radiation temperature near 200 eV for the low-drive and 300 eV for the high drive experiments. In both cases the idea is to drive a single strong shock through the plastic target and measure a locus of Hugoniot points as the shock propagates through the target.

The method for analyzing the radiography for the low-drive experiments in described in Ref. 6. The underlying assumption for the low-drive analysis is that the measured opacity κ for the cold material is unchanged for pressures below about 100 Mbar and therefore a measurement of $\rho * \kappa$ gives you a measurement of the density ρ. However as the temperature and pressure increases for the high-drive experiments the K-shell electrons of boron and carbon start ionizing and the opacity κ starts falling. As we will show later the opacity is well correlated with the K-shell occupation and as we reach interesting regimes where the K-shell occupation affects the EOS we also are in the regime where the opacity is changing.

## 3. Opacity along the boron Hugoniot

In the Gbar experiments we are trying to measure the Hugoniot of boron, plastic, and diamond at pressures from 20 Mbar to 1 Gbar. The low-Z opacities used to model the early Gbar experiments [4] at LLNL come from the OPAL opacity tables [27-30]. However there are issues with these tables due to lack of data at the back-lighter energy that are discussed in Ref. 31 and we do not include the OPAL tables in the comparisons. The alternative opacity tables are the XSN tables developed half a century ago by Lokke and Grasberger [9,10]. XSN is based on an average atom model [11].

When we plot the opacity of boron at 9 keV versus pressure along the Hugoniot using Purgatorio-based Livermore EOS table X52 [25] one sees the opacity from the XSN table, as shown by the dotted line in Fig. 1, converge to a value at low pressure that is about 24% lower than the cold opacity of 1.367 $cm^2/g$ from the Henke table [7]. The corresponding temperatures and densities along the Hugoniot from EOS table X52 are given in Table 1. The issues with the default OPAL opacity table and the lack of other available opacity tables other than XSN motivated us to compare the opacity using different methods such as the Average Atom (AVAT) method from Notre Dame and detailed configuration accounting method (DCA) from LLNL. For many years the average-atom technique has been used to calculate the ionization conditions and absorption spectra of plasma under a wide range of conditions. For finite temperatures and densities the AVAT code calculates a statistical population of one-electron orbitals in the plasma. See Refs. [15-16] for more details. The detailed configuration accounting (DCA) method is described in Refs. [17-18]. DCA treats the plasma as a mixture of atoms in discrete ionization states, thereby giving a more realistic description of individual lines and absorption edges. For this work we use a simple DCA model that identifies levels by quantum number. The photo-ionization cross sections in DCA come from the classical Kramer formulas [32] with the Stewart-Pyatt model [33] used for ionization potential lowering. This is adequate for the K-shell since there is only the 1s orbital in quantum level n = 1. For the free-free component of the opacity, DCA uses the classical inverse Bremstrahlung modified by the free-free Gaunt factor from Karzas and Latter [34] which was based on Coulomb-distorted wave functions. When we look at the AVAT and DCA results in Fig. 1 we observe similar results within 10%. Given the differences between the XSN, AVAT, and DCA results an effort was undertaken to create a new super transition array (STA) based opacity table, shown in blue. The STA method is a powerful technique to model plasmas that accounts for all possible bound-bound radiative transitions and is one method we

have available for creating new opacity models. One sees very similar behavior between AVAT, DCA and STA results in Fig. 1. When analyzing the radiograph it is important to understand at what pressure the opacity starts to vary from the cold opacity and to know how the opacity changes as the pressure and temperature increases. To eliminate the small absolute differences in the opacity at low temperature we plot the normalized opacities for B at 9 keV vs pressure along the Hugoniot in Fig. 2. One sees good agreement with the AVAT opacity falling off slightly faster than STA and DCA falling off the slowest. Figure 3 plots the ratio of the normalized opacity at 9 keV for DCA and AVAT relative to STA. Over the entire range up to 1500 Mbar the opacities agree within -6% to +8%. While this is good agreement any uncertainty in the opacity manifest itself into a similar uncertainty in the density when unfolding radiographic data to measure the Hugoniot (Pressure vs density) for a material such as boron in the high pressure Gbar EOS experiments. Since there are many uncertainties associated with trying to measure the density in the experiments to a few per cent we want to reduce the uncertainty in the measured density associated with the opacity to less than 1%. Keep in mind that when the experiments measure the product of $\rho * \kappa$ from the transmission measurement a 1% change in the opacity $\kappa$ gives a 1% change in the inferred density $\rho$ for a given value of the transmission. Therefore we decided to look in more detail at the opacity and understand the differences between the methods.

**4. Comparing opacity models for four times compressed boron**

Figure 4 shows pressure vs compression along the Hugoniot of boron from the Purgatorio-based Livermore EOS table X52 [25]. The initial density is assumed to be 2.463 g/cc. One quickly sees that the density reaches four times compressed at 200 Mbar and varies less than 10% as the pressure climbs to 1.5 Gbar. Table 1 shows the density, temperature and pressure along the X52 Hugoniot as well as the opacity calculated using the STA method. We can see in Table 1 that the pressure nicely tracks the temperature and that the pressure in Mbar is roughly 4-5 times the temperature in eV as the pressure gets above 200 Mb. We can also look at the opacity calculated by the STA code along the Hugoniot. It stays quite static near the cold opacity value of 1.367 $cm^2/g$ from the Henke table [7] until the pressure climbs above 100 Mbar. We also list the opacity for four times compressed boron at the same temperatures and one observes that the opacity is very similar to the value along the Hugoniot. In the rest of the paper we focus on comparing different opacity models for four times compressed boron versus temperature. We do this for two reasons.

First the ionization and opacity are driven by the temperature. Second, at a given temperature and density the pressure will be different using different EOS tables which makes plots versus pressure dependent on the EOS model. For this work we want to focus on the opacity differences independent of the pressure calculated by the EOS models.

The opacity calculation consists of three terms, bound-bound absorption from resonant transitions, bound-free absorption from photoionization of electrons, and free-free absorption from inverse Bremmstrahlung. In this paper we are looking at the opacity at the 9 keV back-lighter energy used in the Gar experiments so there are no bound-bound transitions at this high energy. Figure 5 shows the bound-free opacity vs temperature for four times compressed boron for calculations done with the STA, DCA, and AVAT methods. The bound-free opacity dominates the free-free opacity shown in Fig. 6 until very high temperatures. One observes that all three methods have very similar results for the bound-free opacity component. At 10 eV the STA opacity is about 2% lower than AVAT but varies from 6.3% higher at 100 eV to 2.5% higher at 200 eV to 1.3% lower at 300 eV. The DCA results start about 1% higher than AVAT and stay about 10% higher over the range from 100 to 200 eV.

Figure 6 shows the free-free opacity component vs temperature for four times compressed boron used by the STA and DCA methods to calculate the total opacity. The free-free component is much smaller than the bound-free until we get to high temperatures. For DCA the free-free component is 2.3% of the bound-free while for STA it is 9.2% of the bound-free component at 10 eV. However the dependence on temperature is very different where the free-free becomes quite constant at high temperature while the bound-free continues to fall as the temperature rises and the plasma ionizes. One also notices quite different behaviour between the model used in the STA and DCA calculations. DCA and AVAT use the same model of the classical inverse Bremstrahlung modified by the free-free Gaunt factor from Karzas and Latter [34] which was based on Coulomb-distorted wave functions. STA has several different options with the default being a phase amplitude method shown in Fig. 6. Clearly it is important to understand which model is correct especially as this affects the total opacity at low temperature and how it converges to the cold opacity used as the baseline opacity. These methods will be compared in more detail in a future publication.

## 5. Correlation of opacity and K-shell occupation

For four times compressed boron the only orbital that is occupied in the STA, DCA, and AVAT calculations is the 1s orbital. One therefore expects that the bound-free opacity to be strongly correlated with the K-shell occupation of the 1s orbital. To address this we looked at the ratio of the bound-free opacity to the K-shell occupation where we normalized the ratio to one at the lowest temperature of 10 eV. Figure 7 plots the normalized ratio vs temperature for the STA, DCA, and AVAT calculations. One observes that the ratio varies from 1 at low temperature to a value of 1.186 at 400 eV for AVAT and almost identical results for DCA and STA. One observes that DCA and AVAT have a very similar shape across the entire range of temperatures while the STA results have a somewhat different shape. As explained in Ref . 16 using the average atom method one expects the ratio to change because the opacity at low temperatures is dominated by the photo-ionization of the two electron state, $1s^2$, while at high temperature photo-ionization is dominated by the photo-ionization of the single electron 1s state. The photo-ionization cross section of hydrogen-like boron has a higher photo-ionization edge and a higher cross section for 9 keV photons by about 20% as reflected in the figure. To better illustrate this correlation Fig. 8 plots the normalized ratio of bound-free opacity to K-shell fraction vs the K-shell fraction for Average Atom (AVAT) calculations. If you fit this curve to a straight line one gets the ratio = $1.2056 - 0.20195*K_{frac}$ where ratio is the normalized ratio of bound-free opacity to K-shell fraction and $K_{frac}$ is the K-shell fraction. One can then calculate a bound-free opacity using Eq. 1

$$\kappa_{BF} = \kappa_{BF0} * K_{frac} * [1.2056 - 0.20195* K_{frac}] \quad (1)$$

where $\kappa_{BF0}$ = 1.2416 $cm^2/g$ for the average atom opacity at 10 eV. Using this formula we can calculate the bound-free opacity to an accuracy of 0.6% over the entire temperature range from 10 – 500 eV. This suggests that with knowledge of the K-shell fraction together with the ratio of the hydrogenic to helium-like photoionization cross sections one can construct the bound-free opacity very accurately.

## 6. Calculating K-shell occupations

Inspired by the above realization we undertook an effort to calculate the K-shell fractions using a variety of density functional theory (DFT) methods that are used to create Equation of State models. One concern and goal going forward is to construct self-consistent EOS and opacity models as opposed to the current approach where EOS and opacity are treated separately. We

looked at three different methods, ONCV, PURGV, and MECCA. PURGV is the Purgatory code that uses a relativistic average atom approach [21,22]. ONCV denotes a pseudopotential method that solves the Kohn-Sham equation [35] using an all-electron optimized norm-conserving Vanderbilt pseudopotential [23-25] and Perdew-Burke-Ernerhof (PBE) [36] functional for exchange-correlation interactions between electrons. The K-shell occupations at each temperature are computed from averaging a set of 10 snapshots taken from the first-principles isochore simulations [25]. The Mermin functional [37] is applied to describe the fractional occupancy of electronic orbitals due to the ionic temperature. Therefore, the ONCV results represent the effect of ionic thermal motions on the K-shell occupations. MECCA is the Multiple-scattering Electronic-structure Calculation for Complex Applications code that uses an all-electron Green's function Korringa-Kohn-Rostoker method [18,19]. As implemented it is a static DFT code that does not sample the ionic degrees explicitly.

With each of these methods we projected the wave functions onto a 1s orbital to estimate the K-shell occupation. Figure 9 shows the K-shell fraction for all six methods vs temperature for four times compressed boron over the range from 10 – 150 eV. MECCA, ONCV, and PURGV all are in excellent agreement with the results from AVAT. One can see that STA and DCA have similar shapes but do not ionize as quickly as the other methods. In Fig. 10 we extend the range from 150 – 400 eV and observe that the STA results converge with the other four methods while the DCA results consistently stay a little higher which is consistent with the DCA opacity being about 10% higher than the average atom results. This comparison gives us confidence that our newest STA calculations are consistent with other methods. However it does point out that to calculate opacities to better than 10% accuracy we need to reconcile the differences between the various methods.

## 7. Conclusions

In this paper we look at how the opacity of boron at 9 keV changes at high pressures and temperatures. Understanding this is vital to unfolding the density in the shock front of equation of state (EOS) experiments as pressures exceed 100 Mbar and reach into the Gbar regime. We compare opacity results between a number of methods including the XSN opacity tables, super transition array (STA), average atom (AVAT) calculations, and detailed configuration accounting (DCA) methods. We show how the data from the XSN tables have opacities that are lower than

the cold opacities by more than 20% at low temperatures and fall off slower than the other methods at higher pressures and how the STA, AVAT, and DCA calculations agree within +-8% for pressures along the Hugoniot up to 1500 Mbar. We examine how the changing opacity is correlated with the K-shell occupation using the STA, AVAT, and DCA opacity methods and density functional theory (DFT) methods such as MECCA, Purgatorio (PURGV), and an optimized density functional theory (ONCV) used to build equation of state tables. We show excellent agreement between the three DFT methods and the Average Atom approach with small differences with STA and DCA opacity methods. We also examine the relative contribution of free-free opacity to the overall opacity that is dominated by bound-free absorption. We show how different methods give results that vary by as much as a factor of four for the free-free at low temperatures and pressures. While we have good agreement between different methods at the 10% level more work is needed to understand the differences between the methods so as to reduce the uncertainty in the density measured in the EOS experiments due to the uncertainty in the opacity to less than 1%. All these same issues apply to the opacity of carbon in the Gbar experiments that measure the EOS of plastic and diamond.

**Acknowledgements.** This work was performed under the auspices of the U.S. Department of Energy by Lawrence Livermore National Laboratory under Contract DE-AC52-07NA27344.

## References

[1] L. Stixrude, Phys. Rev. Lett. **108** (2012) 055505.
[2] S. Seager, et al., Astrophys. J. **669** (2007) 1279.
[3] V. E. Fortov, Extreme States of Matter on Earth and in the Cosmos, Springer-Verlag, Heidelberg, 2011, p. 224.
[4] A. L. Kritcher, T. Döppner, D. Swift, J. Hawreliak, G. Collins, J. Nilsen, B. Bachmann, E. Dewald, D. Strozzi, S. Felker, O.L. Landen, O. Jones, C. Thomas, J. Hammer, C. Keane, H.J. Lee, S. H. Glenzer, S. Rothman, D. Chapman, D. Kraus, P. Neumayer, R.W. Falcone, "Probing matter at Gbar pressures at the NIF," HEDP **10** (2014) 27 – 34.
[5] T. Döppner, D. C. Swift, A. L. Kritcher, B. Bachmann, G.W. Collins, D.A. Chapman, J. Hawreliak, D. Kraus, J. Nilsen, S. Rothman, L. X. Benedict, E. Dewald, D. E. Fratanduono, J. A. Gaffney, S. H. Glenzer, S. Hamel, O. L. Landen, H. J. Lee, S. LePape, T. Ma, M.J. MacDonald, A. MacPhee, D. Milathianaki, M. Millot, P. Neumayer, P. A. Sterne, R. Tommasini, R. W. Falcone, "Absolute equation-of-state measurements for polystyrene from

25 - 60 Mbar using a spherically converging shock wave," Phys. Rev. Lett. **121** (2018) 025001.
[6] Damian C. Swift, Andrea L. Kritcher, James A. Hawreliak, Amy Lazicki, Andrew MacPhee, Benjamin Bachmann, Tilo Döppner, Joseph Nilsen, Gilbert W. Collins, Siegfried Glenzer, Stephen D. Rothman, Dominik Kraus, and Roger W. Falcone, "Absolute Hugoniot measurements from a spherically-convergent shock using x-ray radiography," Rev. Sci. Instr. **89** (2018) 053505.
[7] B.L. Henke, E.M. Gullikson, J.C. Davis, At. Data Nucl. Data Tables **54** (1993) 181. See boron data online at http://henke.lbl.gov/optical_constants/sf/b.nff
[8] Andrea L. Kritcher et al., "Laboratory equation of state measurements of carbon atmospheres of white dwarf stars," LLNL report LLNL-JRNL-769585 (July 2019).
[9] W. A. Lokke and W. H. Grasberger, "XSNQ-U: a non-LTE emission and absorption coefficient subroutine," Lawrence Livermore National Laboratory report UCRL-52276 (January 6, 1977).
[10] R. V. Jensen, D. E. Post, W. H. Grasberger, C. B. Tarter, and W. A. Lokke, "Calculations of impurity radiation and its effects on tokamak experiments," Nuclear Fusion **17** (1977) 1187 – 1196.
[11] Greg Pollak. "Detailed physics of XSN-U opacity package", Technical report LA-UR-90-2423, Los Alamos National Laboratory, Los Alamos, NM, (January1990).
[12] A. Bar-Shalom, et al., Phys. Rev. A40 (1989) 3183.
[13] A. Bar-Shalom, et al., Phys. Rev. E51 (1995) 4882.
[14] Brian G. Wilson, Carlos A. Iglesias, and Mau H. Chen, "Partially resolved super transition array method," HEDP 14 (2015) 67 – 73.
[15] W. R. Johnson, C. Guet, and G. F. Bertsch, "Optical properties of plasmas based on an average-atom model," JQRST **99** (2006) 327-340.
[16] Walter R. Johnson and Joseph Nilsen, "Opacity of shock-heated boron plasmas," HEDP **31** (2019) 92-98.
[17] Y. T. Lee, "A model for ionization balance and L-shell spectroscopy of non-LTE plasmas," J. Quant. Spectrosc. Radiat. Transfer 38 (1987) 131 – 145.
[18] H. A. Scott and S. B. Hansen, "Advances in NLTE modeling for integrated simulations," HEDP 6 (2010) 39 – 47.
[19] B. G. Wilson, D. D. Johnson, A. Alam, "Multi-center electronic structure calculations for plasma equation of state, HEDP **7** (2011) 61-70.
[20] J. A. Gaffney et al., "A review of equation-of-state models for inertial confinement fusion materials," HEDP 28 (2018) 7-24.
[21] B. Wilson, V. Sonnad, P. Sterne, and W. Isaacs, J. Quant. Spectrosc. Radiat. Transfer 99 (2006) 658.
[22] P. Sterne, S. Hansen, B. Wilson, and W. Isaacs, High Energ. Dens. Phys. 3 (2007) 278.
[23] D. R. Hamann, Phys. Rev. B 88 (2013) 085117.
[24] D. R. Hamann, Phys. Rev. B 95 (2017) 239906.

[25] S. Zhang et al., "Theoretical and experimental investigation of the equation of state of boron plasmas," Phys. Rev. E **98** (2018) 023205.
[26] Joseph Nilsen, Andrea L. Kritcher, Madison E. Martin, Robert E. Tipton, Heather D. Whitley, Damian C. Swift, Tilo Döppner, Benjamin L. Bachmann, Amy E. Lazicki, Natalie B. Kostinski, Brian R. Maddox, Gilbert W. Collins, Siegfried H. Glenzer, and Roger W. Falcone, "Understanding the effects of radiative preheat and self-emission from shock heating on equation of state measurement at 100's of Mbar using spherically converging shock waves in a NIF hohlraum," Matter Radiat. Extremes 5 (2020) 018401.
[27] C. A. Iglesias, F. J. Rogers, and B. G. Wilson, Astrophys. J. Lett. **322** (1987) L45.
[28] F. J. Rogers, B. G. Wilson, and C. A. Iglesias, Phys. Rev. A **38** (1988) 5007.
[29] C. A. Iglesias and F. J. Rogers Astrophys. J. **464** (1996) 943.
[30] Franck Delahaye, Carlo Maria Zwoelf, Claude J. Zeippen, Claudio Mendoza, "IPOPv2 online service for the generation of opacity tables," JQSRT 171 (2016) 66-72.
[31] Joseph Nilsen et al.," Comparing opacity tables for boron and plastic with average atom calculations at the 9 keV back lighter energy used in radiography to measure the equation of state Hugoniot at pressures up to a Gbar," LLNL-report in preparation (2020).
[32] H. A. Kramer, Phil. Mag. 271 (1923) 836.
[33] J. C. Stewart and K. D. Pyatt, "Lowering of ionization potentials in plasmas," Ap. J. 144 (1966) 1203-1211.
[34] W. J. Karzas and R. Latter, "Electron radiative transitions in a coulomb field", Ap. JS 6 (1961) 167 – 212.
[35] W. Kohn and L. J. Sham, "Self-consistent equations including exchange and correlation effects," Phys. Rev. 140 (1965) A1133.
[36] J. P. Perdew, K. Burke, and M. Ernzerhof, "Generalized gradient approximation made simple", Phys. Rev. Lett. 77 (1996) 3865.
[37] N. D. Mermin, "Thermal properties of the inhomogeneous electron gas," Phys. Rev. 137 (1965) A1441.

Table 1: Plasma parameters and STA opacity along the Hugoniot X52 for boron. Also is a separate calculation of the STA opacity for four times compressed boron at the temperature used for the Hugoniot and the ratio of the opacity along the Hugoniot to the opacity at four times compressed boron at the same temperature.

| Density | Compression | Temperature | Pressure | Opacity(X52) | Opacity(4x) | Ratio |
|---|---|---|---|---|---|---|
| g/cc | | eV | Mbar | $cm^2/g$ | $cm^2/g$ | |
| 7.327 | 2.975 | 10.04 | 30.28 | 1.356 | 1.369 | 0.991 |
| 8.147 | 3.308 | 19.91 | 60.70 | 1.352 | 1.360 | 0.994 |
| 8.651 | 3.513 | 30.03 | 94.30 | 1.345 | 1.350 | 0.996 |
| 9.121 | 3.703 | 40.10 | 132.38 | 1.331 | 1.334 | 0.997 |
| 9.361 | 3.801 | 45.29 | 154.23 | 1.315 | 1.318 | 0.998 |
| 9.553 | 3.879 | 49.62 | 173.57 | 1.303 | 1.305 | 0.998 |
| 9.783 | 3.972 | 55.20 | 199.79 | 1.276 | 1.277 | 1.000 |
| 9.980 | 4.052 | 60.48 | 225.81 | 1.252 | 1.251 | 1.001 |
| 10.139 | 4.116 | 65.26 | 250.22 | 1.224 | 1.221 | 1.003 |
| 10.289 | 4.177 | 70.42 | 277.30 | 1.192 | 1.186 | 1.005 |
| 10.428 | 4.234 | 75.98 | 307.26 | 1.153 | 1.145 | 1.007 |
| 10.531 | 4.276 | 80.75 | 333.44 | 1.122 | 1.112 | 1.009 |
| 10.625 | 4.314 | 85.82 | 361.66 | 1.086 | 1.074 | 1.012 |
| 10.709 | 4.348 | 91.21 | 392.04 | 1.050 | 1.035 | 1.014 |
| 10.766 | 4.371 | 95.47 | 416.32 | 1.021 | 1.004 | 1.017 |
| 10.817 | 4.392 | 99.93 | 441.93 | 0.992 | 0.973 | 1.019 |
| 10.863 | 4.410 | 104.59 | 468.89 | 0.959 | 0.939 | 1.022 |
| 10.902 | 4.426 | 109.48 | 497.27 | 0.928 | 0.906 | 1.025 |
| 10.947 | 4.445 | 116.35 | 537.38 | 0.882 | 0.858 | 1.028 |
| 10.974 | 4.456 | 121.78 | 569.25 | 0.849 | 0.823 | 1.031 |
| 10.989 | 4.462 | 125.55 | 591.36 | 0.826 | 0.800 | 1.033 |
| 11.008 | 4.469 | 131.41 | 625.85 | 0.793 | 0.765 | 1.035 |
| 11.017 | 4.473 | 135.47 | 649.77 | 0.769 | 0.741 | 1.037 |
| 11.028 | 4.477 | 141.80 | 687.05 | 0.735 | 0.707 | 1.040 |
| 11.032 | 4.479 | 146.18 | 712.86 | 0.714 | 0.685 | 1.042 |
| 11.035 | 4.480 | 150.70 | 739.47 | 0.692 | 0.663 | 1.044 |
| 11.034 | 4.480 | 160.16 | 795.10 | 0.643 | 0.613 | 1.049 |
| 11.027 | 4.477 | 170.21 | 854.07 | 0.596 | 0.565 | 1.055 |
| 11.014 | 4.472 | 180.89 | 916.54 | 0.550 | 0.520 | 1.058 |
| 10.995 | 4.464 | 192.24 | 982.66 | 0.506 | 0.477 | 1.061 |
| 10.959 | 4.449 | 210.62 | 1089.02 | 0.446 | 0.419 | 1.064 |
| 10.914 | 4.431 | 230.76 | 1204.61 | 0.391 | 0.367 | 1.066 |
| 10.873 | 4.414 | 249.00 | 1308.53 | 0.350 | 0.328 | 1.067 |
| 10.819 | 4.393 | 272.80 | 1443.04 | 0.306 | 0.287 | 1.066 |
| 10.782 | 4.378 | 289.92 | 1539.13 | 0.280 | 0.262 | 1.067 |
| 10.735 | 4.358 | 312.84 | 1667.01 | 0.246 | 0.230 | 1.069 |
| 10.696 | 4.343 | 332.48 | 1775.94 | 0.225 | 0.211 | 1.068 |
| 10.640 | 4.320 | 364.26 | 1951.32 | 0.198 | 0.186 | 1.066 |

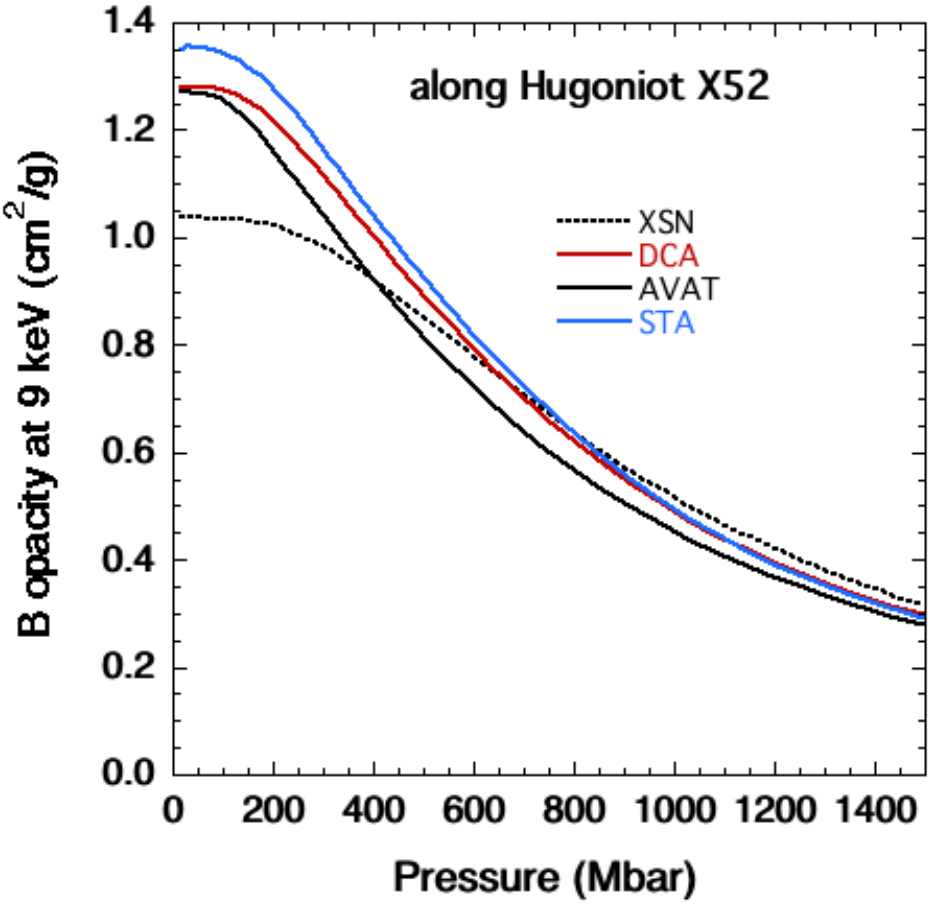


Fig. 1. Boron opacity at 9 keV versus pressure along the Livermore X52 Hugoniot comparing four different methods. Results are from a legacy XSN table (black dotted), DCA (red), AVAT (black), and STA (blue). The corresponding temperatures and densities along the Hugoniot from EOS table X52 are given in Table 1.

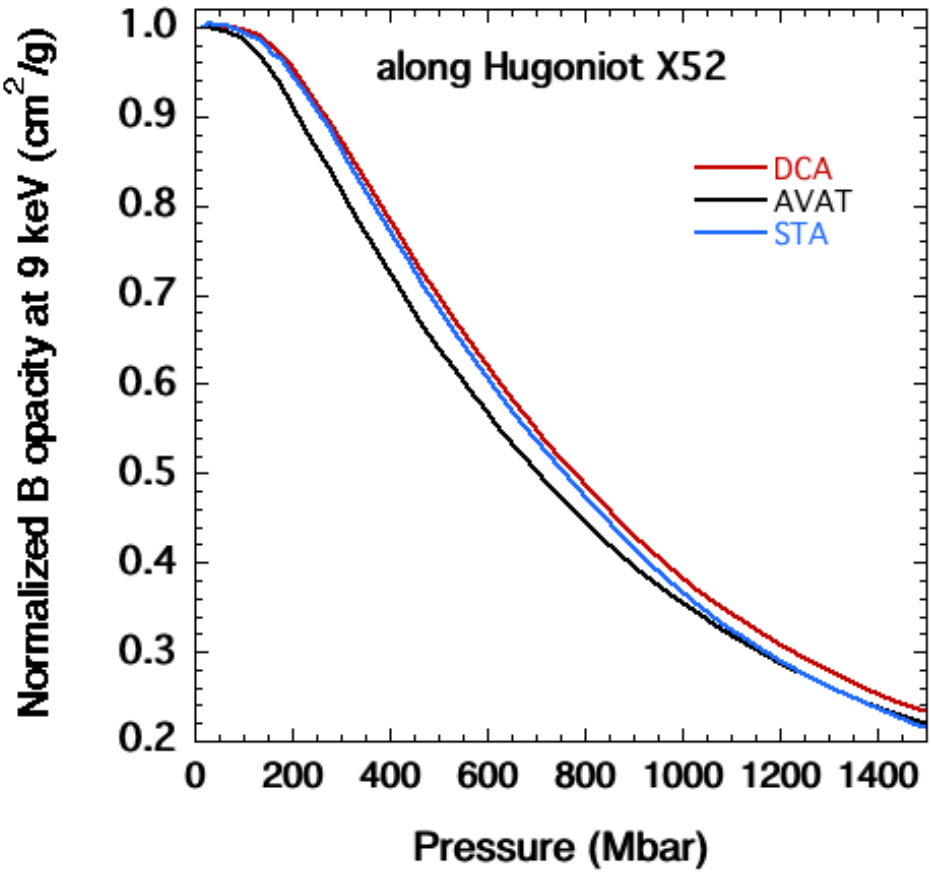


Fig. 2. Boron opacity at 9 keV normalized to one at coldest value (5 eV) versus pressure along the Livermore X52 Hugoniot comparing three different methods. Results are from DCA (red), AVAT (black), and STA (blue).

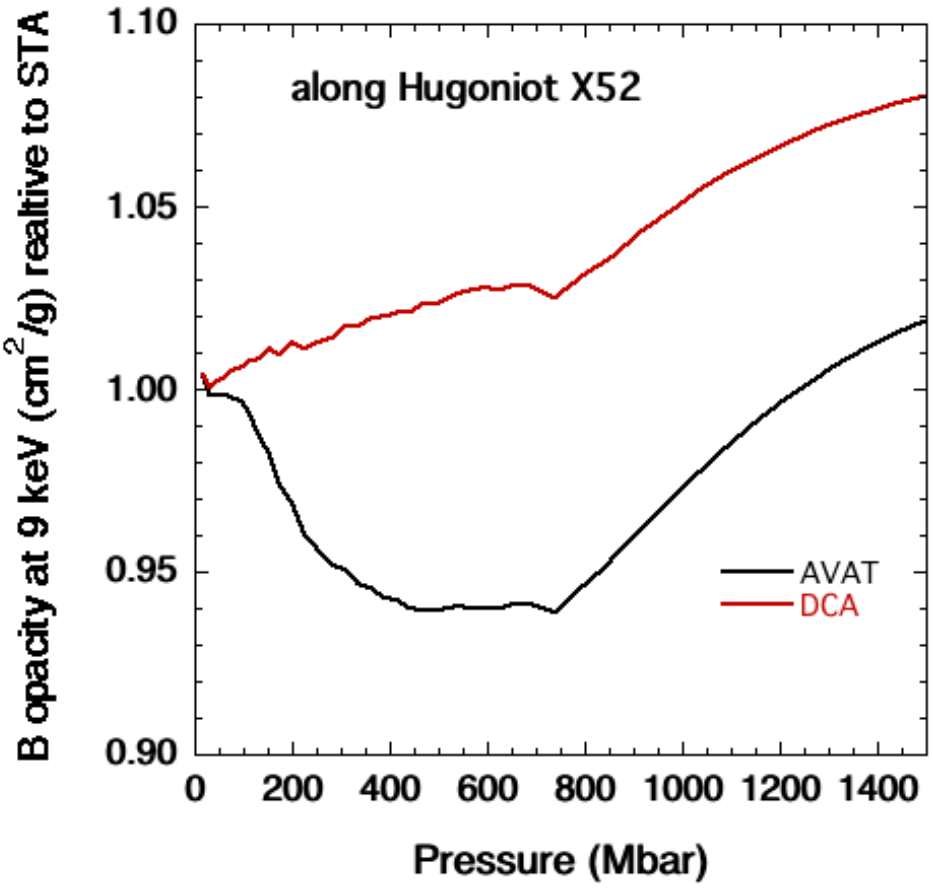


Fig. 3. Boron opacity at 9 keV for AVAT (black) and DCA (red) relative to the STA opacity versus pressure along the Livermore X52 Hugoniot.

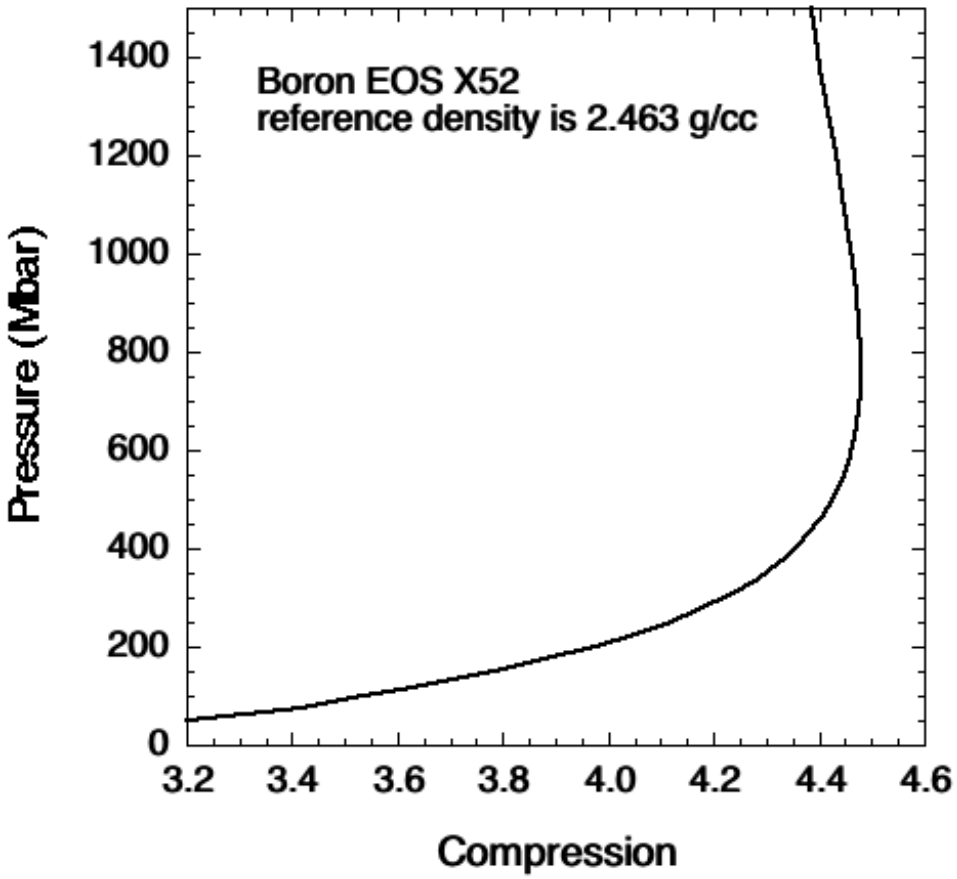


Fig. 4. Pressure versus compression along the Livermore X52 Hugoniot for Boron. The reference density for boron is 2.463 g/cc. The corresponding temperatures and densities along the Hugoniot from EOS table X52 are given in Table 1.

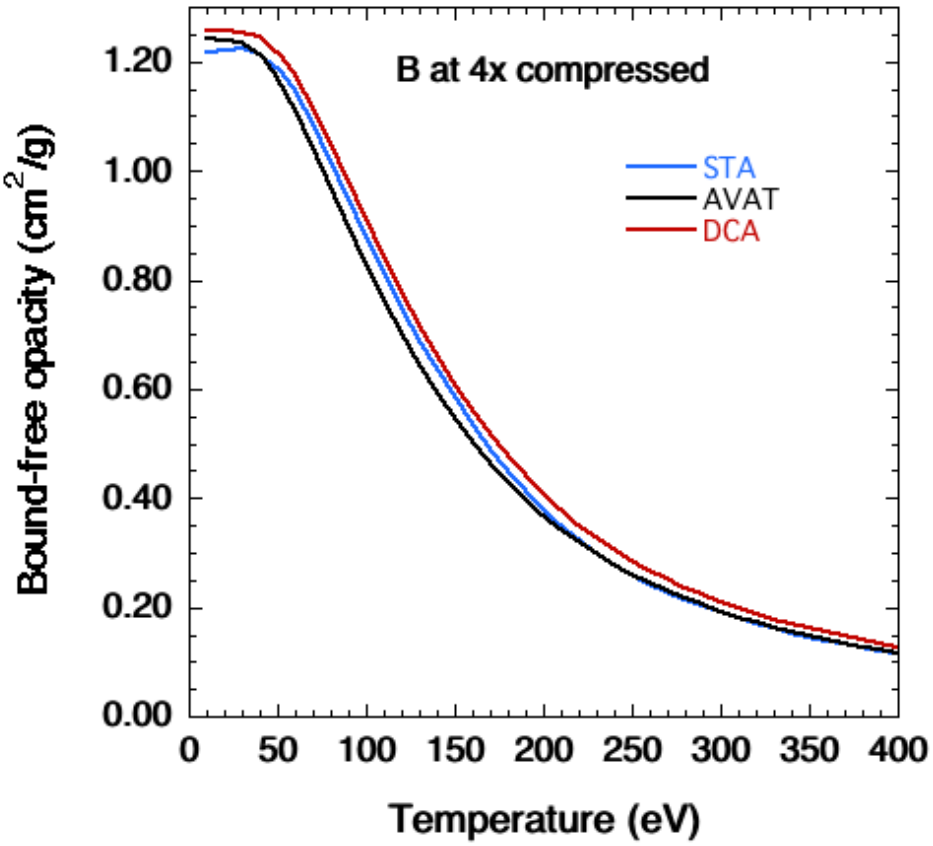


Fig. 5. Bound free component of the B opacity at 9 keV versus temperature for four times compressed boron. Shown are results from three methods, STA, AVAT, and DCA. The reference density for boron is 2.463 g/cc.

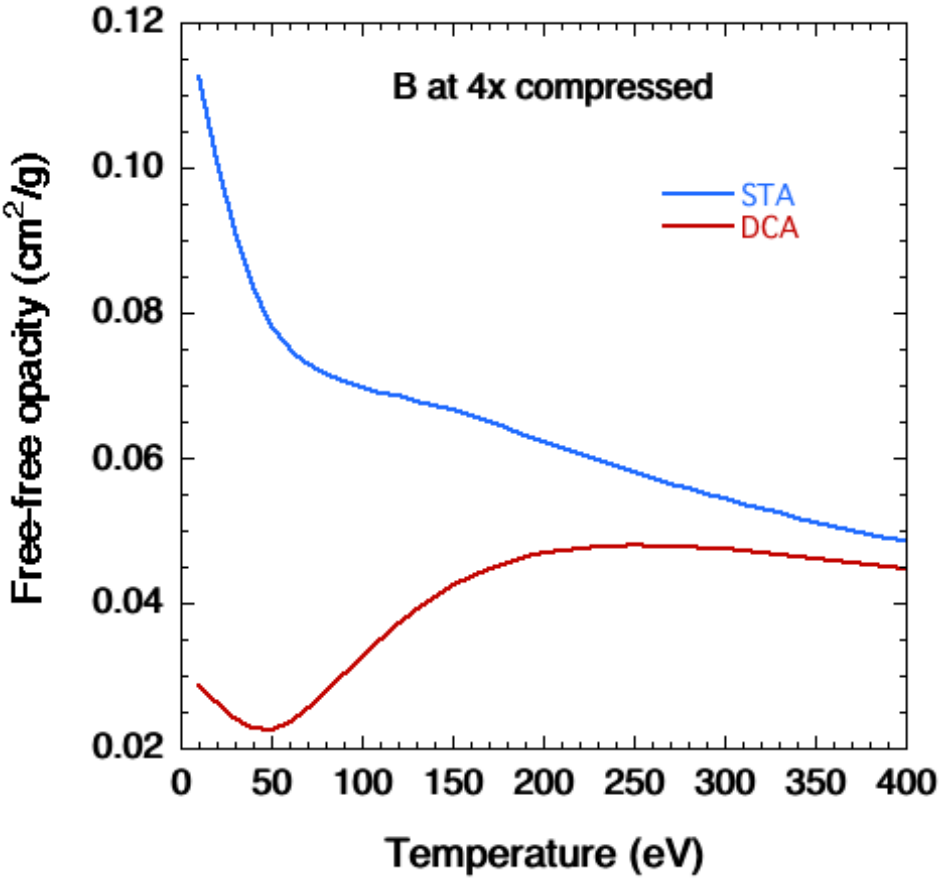


Fig. 6. Free-free component of the B opacity at 9 keV versus temperature for four times compressed boron. Shown are results used by two methods, STA and DCA. STA result using the phase amplitude option is shown for computing free-free while DCA is using a classical result modified by the Karzas-Latter gaunt factor. The reference density for boron is 2.463 g/cc.

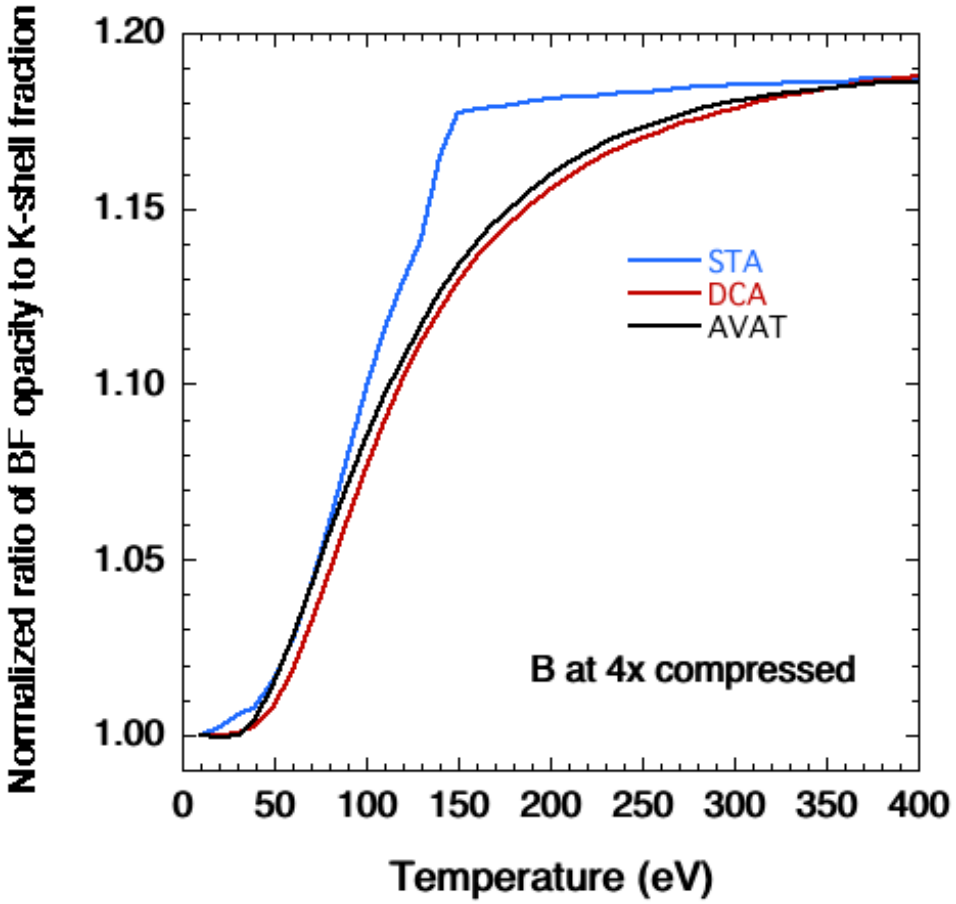


Fig. 7. Normalized ratio of the bound-free opacity at 9 keV to the fractional K-shell occupation vs temperature for four times compressed boron. Shown are results used by three methods, STA, DCA, and AVAT. The reference density for boron is 2.463 g/cc.

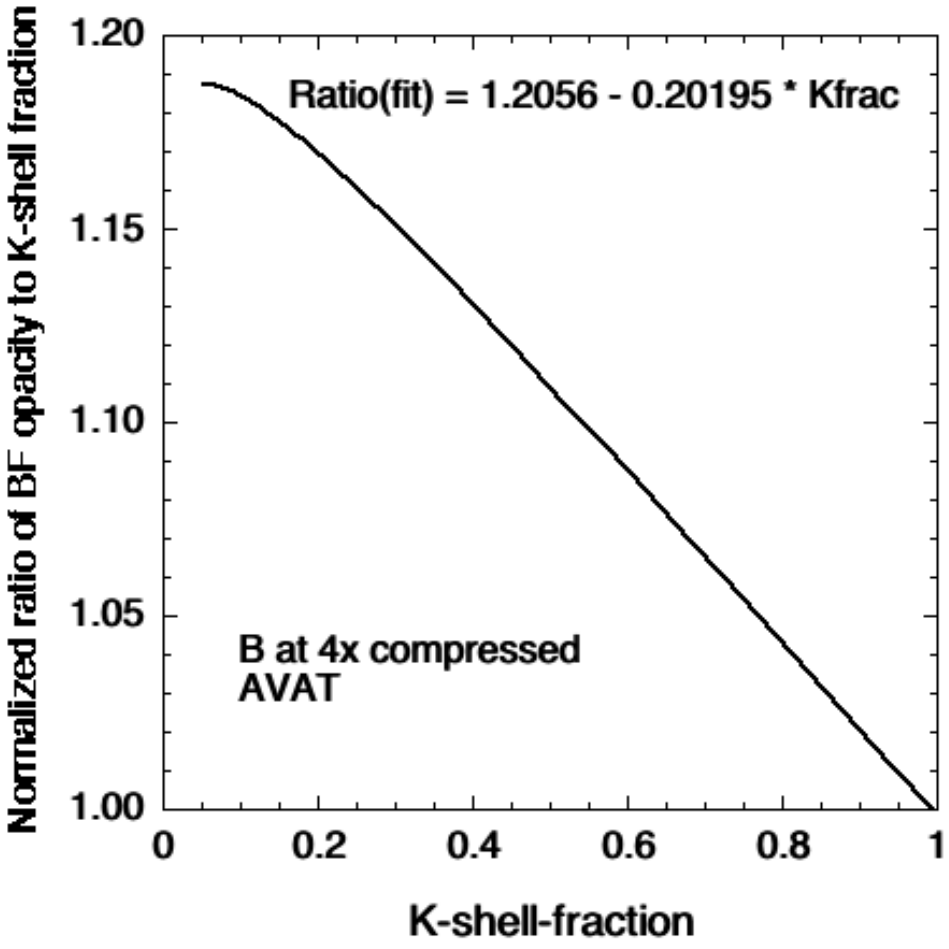


Fig. 8. Normalized ratio of the bound-free opacity at 9 keV to the fractional K-shell occupation vs the fractional K-shell occupation for four times compressed boron. Shown are results using the average atom method (AVAT). The reference density for boron is 2.463 g/cc.

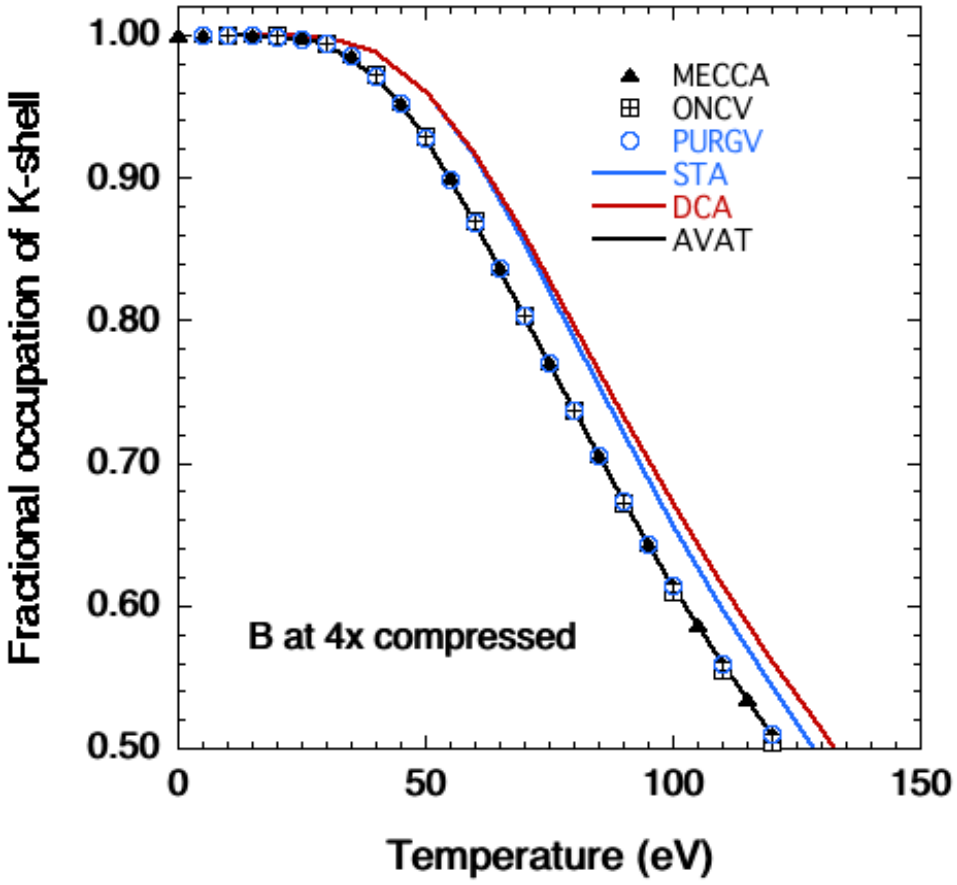


Fig. 9. Fractional K-shell occupation vs temperature for four times compressed boron. Shown are results using three opacity methods from STA, DCA, and AVAT and three equation of state code methods from MECCA, ONCV, and PURGV. The reference density for boron is 2.463 g/cc.

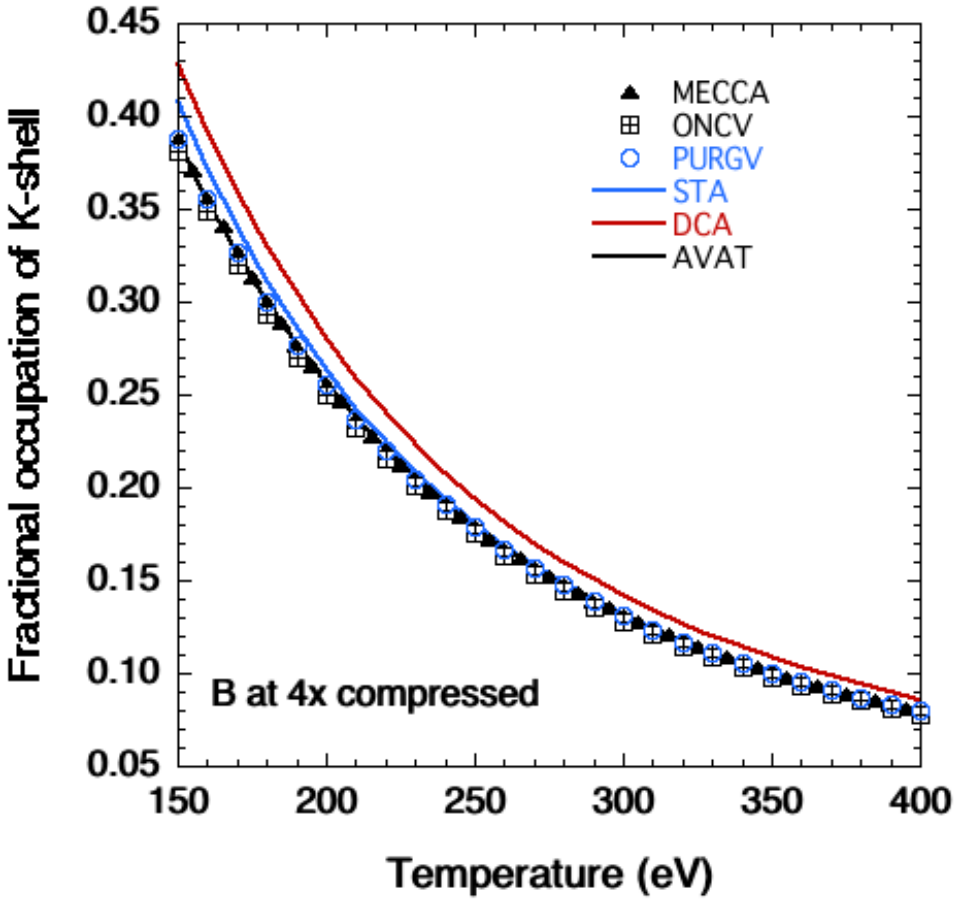


Fig. 10. Fractional K-shell occupation vs temperature for four times compressed boron. Shown are results using three opacity methods from STA, DCA, and AVAT and three equation of state code methods from MECCA, ONCV, and PURGV. The reference density for boron is 2.463 g/cc.